

## Scaling violations in electromagnetic and neutrino scattering

Inga Karliner and Jeremiah D. Sullivan

*Department of Physics, University of Illinois at Urbana-Champaign, Urbana, Illinois 61801*

(Received 2 June 1978)

Scaling violations in neutrino and antineutrino charged current interactions are studied using phenomenological power and logarithmic descriptions determined from  $eN$  and  $\mu N$  scattering. Results for the two descriptions are very similar to one another and to the predictions from the full machinery of asymptotically free quantum chromodynamics. The accuracy of presently available  $\nu N$  and  $\bar{\nu} N$  experimental results, and in some cases the large spread between different experiments, permits only a qualitative test of the expectations for scale breaking at this time.

### I. INTRODUCTION

This work discusses scaling violations in high-energy neutrino and antineutrino charged-current interactions. This topic has been treated already by a number of authors within the detailed formalism of asymptotically free quantum chromodynamics (QCD).<sup>1</sup> The approach presented here is instead entirely phenomenological. We first examine high- $x$  inelastic  $eN$  data<sup>2</sup> and low- $x$  inelastic  $\mu N$  data<sup>3</sup> to fix the size and  $x$  and  $Q^2$  dependence of scale breaking in electromagnetic interactions. We then impose this pattern of scale breaking on inelastic  $\nu N$  and  $\bar{\nu} N$  scattering and study the results. In particular, we examine the energy dependence of  $\sigma^{\nu, \bar{\nu}}/E$ ,  $R_c \equiv \sigma^{\bar{\nu}}/\sigma^{\nu}$ ,  $\langle y \rangle^{\nu, \bar{\nu}}$ , and  $\langle Q^2 \rangle^{\nu, \bar{\nu}}$  using the standard four-flavor quark model with weak and electromagnetic couplings according to the Glashow-Iliopoulos-Maiani pattern.<sup>4</sup>

We consider two different parametrizations of scale breaking, one involving logarithms as suggested by asymptotic freedom, the other power-type suggested by conventional, renormalizable field theories. As we show below, both forms provide acceptable descriptions of the observed scale breaking in inelastic  $eN$  and  $\mu N$  scattering and, moreover, both predict remarkably similar scaling violations in inelastic  $\nu N$  and  $\bar{\nu} N$  processes in the regions currently explored. We also find that the scale violations predicted by our phenomenological approach are quite similar to those predicted for  $\nu N$  and  $\bar{\nu} N$  by the full machinery of asymptotic freedom<sup>1</sup> and are rather insensitive to the particular choice of quark distribution functions.<sup>5</sup> These observations are not entirely surprising since the size of scaling violations predicted by QCD and the behavior of quark densities must in practice be calibrated also by inelastic  $eN$  and  $\mu N$  data.

We find further, in agreement with previous treatments, that the presently available neutrino

and antineutrino results, where there is agreement among the various experiments, are compatible with the expectations from scale breaking obtained from  $eN$  and  $\mu N$ . This comparison is at present largely qualitative, however, since the systematic and statistical errors of available experimental results typically dominate the variations predicted from scale breaking. Finally, we note that the predictions for several of the observables which we study are very sensitive to experimental acceptance cuts. We discuss the difficulties which result from insufficient description of these cuts and from different correcting procedures. The comparison between various experiments as well as with the theory would be greatly facilitated if the data were presented uncorrected for acceptance with the cuts clearly stated.

### II. SCALE BREAKING IN ELECTROPRODUCTION

It is well established that the proper theoretical framework for discussing asymptotic scale breaking is the moment spectrum of the structure functions.<sup>6</sup> The behavior in  $Q^2$  of these moments fingerprints the underlying field theory: conventional, renormalizable field theory versus asymptotically free gauge theories. In spite of this we cannot choose at the present time between these two opinions. As extensive analyses by Tung and collaborators has shown,<sup>7</sup> there is not yet enough range in  $Q^2$  in deep-inelastic  $eN$  and  $\mu N$  experiments to distinguish  $(Q^2)^\gamma$  from  $\gamma' \ln(Q^2)$  with  $\gamma, \gamma'$  small. Both types of scale breaking give acceptable fits to the observed data. We therefore consider both here.

For the  $eN$  ( $\mu N$ ) deep-inelastic case we have, dropping terms of order  $M_N^2/Q^2$ ,

$$\frac{d^2 \sigma'}{dx dy} = \frac{8\pi \alpha^2 M_N E}{Q^2} [xy^2 F_1(x, Q^2) + (1-y)F_2(x, Q^2)], \quad (1)$$

where  $x = -q^2/2p \cdot q = Q^2/2p \cdot q$  and  $y = E_{\text{had}}/E$ . Let us assume, together with many other authors, that it is still meaningful to describe deep-inelastic lepton-hadron production in a quark-parton-model language even in the presence of scale breaking.<sup>1,8</sup> Namely, we consider a  $Q^2$  dependence in the parton-model quark densities, i.e.,

$$F_2^{\gamma p}(x, Q^2) = x \left\{ \frac{4}{9} [u(x, Q^2) + \bar{u}(x, Q^2)] + \frac{1}{9} [d(x, Q^2) + \bar{d}(x, Q^2) + s(x, Q^2) + \bar{s}(x, Q^2)] \right\} \quad (2a)$$

and

$$F_2^{\gamma n}(x, Q^2) = x \left\{ \frac{4}{9} [d(x, Q^2) + \bar{d}(x, Q^2)] + \frac{1}{9} [u(x, Q^2) + \bar{u}(x, Q^2) + s(x, Q^2) + \bar{s}(x, Q^2)] \right\}. \quad (2b)$$

Note that we have neglected the charm content of the nucleon.

We relate  $F_1$  and  $F_2$  by a modified Callan-Gross relation<sup>9</sup>

$$F_2(x, Q^2) = [1 + \mathcal{R}(x, Q^2)] 2xF_1(x, Q^2). \quad (3)$$

Throughout this work we will treat  $\mathcal{R}$  as a constant, independent of  $x$  and  $Q^2$ . This cannot be literally true since current conservation implies that  $\mathcal{R}$  vanishes as  $Q^2 \rightarrow 0$  at fixed  $\nu$ , and the spin- $\frac{1}{2}$  parton model, without scale breaking, demands that  $\mathcal{R} \rightarrow 0$  in the deep-inelastic limit  $Q^2 \rightarrow \infty$  at fixed  $x$ . Unfortunately, the experimental situation regarding  $\mathcal{R}$  remains quite uncertain in spite of enormous effort. (A review, including new SLAC results, is given in Ref. 10). In most of our calculations we use  $\mathcal{R} = 0.14$  for both the proton and the neutron.<sup>11</sup> We will occasionally indicate the sensitivity of our results to the choice of  $\mathcal{R}$ .

The most general form of scale breaking permits a different behavior in  $Q^2$  for each of the quark densities, but such a situation allows no predictions in absence of a detailed theoretical model. Instead, we consider a two component form which can be fitted phenomenologically, namely

$$q_v(x, Q^2) = q_v(x, Q_0^2) B^v(x, Q^2, Q_0^2) \quad (4)$$

for valence quarks, and

$$q_c(x, Q^2) = q_c(x, Q_0^2) B^c(x, Q^2, Q_0^2) \quad (5)$$

for sea quarks. Thus

$$\begin{aligned} u(x, Q^2) &= u_v(x, Q_0^2) B^v(x, Q^2, Q_0^2) \\ &\quad + u_c(x, Q_0^2) B^c(x, Q^2, Q_0^2), \\ d(x, Q^2) &= d_v(x, Q_0^2) B^v(x, Q^2, Q_0^2) \\ &\quad + d_c(x, Q_0^2) B^c(x, Q^2, Q_0^2). \end{aligned} \quad (6)$$

Virtually all of the (scaling) quark-density models

have readily identifiable "valence" and "sea" terms, the latter usually symmetric in flavor. We do not imply that there is a fundamental difference between the valence and sea distributions, rather we regard Eq. (6) as a reasonable but flexible parametrization which can be fit directly to deep-inelastic electroproduction on proton and deuterium targets. This avoids the need for and the accompanying assumptions of the moment expansion of the structure functions, but allows more than single-component scale breaking, as expected on general theoretical grounds. We will discuss below the choice of  $Q_0^2$  and its significance in the two parametrizations that we employ.

We have then, in terms of electroproduction data and quark densities at  $Q_0^2$ ,

$$B^v(x, Q^2, Q_0^2) = \frac{F_2^{\gamma N}(x, Q^2) C_p(x, Q_0^2) - F_2^{\gamma p}(x, Q^2) C_N(x, Q_0^2)}{V_N(x, Q_0^2) C_p(x, Q_0^2) - V_p(x, Q_0^2) C_N(x, Q_0^2)}, \quad (7)$$

$$B^c(x, Q^2, Q_0^2) = \frac{F_2^{\gamma p}(x, Q^2) V_N(x, Q_0^2) - F_2^{\gamma N}(x, Q^2) V_p(x, Q_0^2)}{V_N(x, Q_0^2) C_p(x, Q_0^2) - V_p(x, Q_0^2) C_N(x, Q_0^2)},$$

where

$$F_2^{\gamma N} = \frac{1}{2}(F_2^{\gamma p} + F_2^{\gamma n}),$$

and

$$\begin{aligned} V_N(x, Q^2) &= \frac{5}{18} x [u_v(x, Q^2) + d_v(x, Q^2)], \\ V_p(x, Q^2) &= \frac{1}{9} x [4u_v(x, Q^2) + d_v(x, Q^2)], \\ C_N(x, Q^2) &= \frac{5}{18} x [u_c(x, Q^2) + \bar{u}_c(x, Q^2) \\ &\quad + d_c(x, Q^2) + \bar{d}_c(x, Q^2)] \\ &\quad + \frac{1}{9} x [s(x, Q^2) + \bar{s}(x, Q^2)], \\ C_p(x, Q^2) &= \frac{4}{9} x [u_c(x, Q^2) + \bar{u}_c(x, Q^2)] \\ &\quad + \frac{1}{9} x [d_c(x, Q^2) + \bar{d}_c(x, Q^2) \\ &\quad + s(x, Q^2) + \bar{s}(x, Q^2)]. \end{aligned} \quad (8)$$

Differences in the behavior of  $B^v$  and  $B^c$  will lead to differences in scale breaking for deuterium and proton targets, as well as to differences in the  $Q^2$  dependence of  $F_2$  and  $xF_3$  in neutrino production.

To solve for the  $B(x, Q^2, Q_0^2)$ , we combined the SLAC electroproduction data<sup>2</sup> for  $x \geq 0.10$  with the  $\mu N$  data from Fermilab<sup>3</sup> for  $x < 0.10$ . As of now, these data indicate some but not a large difference between scale breaking for proton and deuterium targets. Much better statistics in the low- $x$  region, particularly for deuterium data, is still needed. Therefore, as a working hypothesis

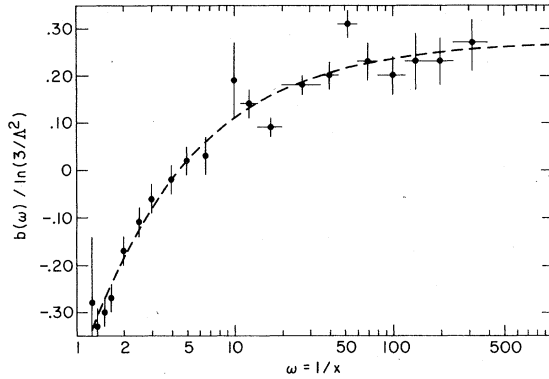


FIG. 1. The quantity  $b(\omega=1/x)$  vs  $\omega$  for logarithmic scale breaking, Eq. (9). The data are obtained from Ref. 2 ( $\omega \leq 10$ ) and Ref. 3 ( $\omega > 10$ ), as described in the text. The curve represents our fit, Eq. (10), with  $Q_0^2 = 3 \text{ GeV}^2$ .

subject to future refinement, we take here  $B^\nu = B^c = B(x, Q^2, Q_0^2)$ .

The overall behavior in  $x$  and  $Q^2$  for a logarithmic  $Q^2$  dependence, suggested by asymptotic freedom, is well fitted by

$$F_2^\gamma(x, Q^2) \equiv B_L(x, Q^2, Q_0^2) F_2^\gamma(x, Q_0^2) \equiv \left[ 1 + b(x) \frac{\ln(Q^2/Q_0^2)}{\ln(Q_0^2/\Lambda^2)} \right] F_2^\gamma(x, Q_0^2). \quad (9)$$

We obtained values of  $b(x)$  by a least-squares fit to the combined SLAC and Fermilab data set in each of the 21  $\omega$  bins ( $\omega = 1/x$ ). The results are shown in Fig. 1 for  $Q_0^2 = 3 \text{ GeV}^2$  and  $\Lambda = 0.400 \text{ GeV}$ . The errors displayed in Fig. 1 reflect only the experimental uncertainties.

It is convenient for our subsequent calculations to have a simple analytic expression for  $b(x)$  which reproduces the experimental values shown in Fig. 1. We find that

$$b(x) = b_0 [1 - (x/x_0)^\alpha], \quad (10)$$

with  $x_0^{-1} = 4.489$ ,  $b_0 = 0.804$  and  $\alpha = 0.6345$  is quite adequate. This parametrization is shown by the dashed curve in Fig. 1.

In our fits to electron and muon data and in our subsequent applications to neutrino processes it is understood that Eq. (9) is to be applied over a limited range of  $Q$ , namely  $Q_0/2 \leq Q \leq 2Q_0$ . To go outside this range the formula is to be applied recursively,<sup>12</sup> e.g., for the range  $2Q_0 \leq Q \leq 4Q_0$ , use

$$F_2^\gamma(x, Q^2) = \left( 1 + b(x) \frac{\ln(Q^2/4Q_0^2)}{\ln(4Q_0^2/\Lambda^2)} \right) \times \left( 1 + b(x) \frac{\ln(4)}{\ln(Q_0^2/\Lambda^2)} \right) F_2^\gamma(x, Q_0^2). \quad (9')$$

Obviously the scale-breaking structure implied by Eq. (9) cannot be carried to very small  $Q^2$  since it will not generate the kinematic zero in  $Q^2$  which  $F_2$  must have.<sup>13</sup> Consequently, in our fitting procedure for electron and muon scattering we use no data below  $Q^2 = 0.45 \text{ GeV}^2$ .

Another scale-breaking fit, advocated by Perkins,<sup>14</sup> and loosely associated with conventional, renormalizable "fixed-point" field theories,<sup>7</sup> employs an  $x$ -dependent power of  $Q^2$ :

$$F_2^\gamma(x, Q^2) \equiv B_P(x, Q^2, Q_0^2) F_2^\gamma(x, Q_0^2) \equiv (Q^2/Q_0^2)^{f(x)} F_2^\gamma(x, Q_0^2). \quad (11)$$

Note that this formula is invariant under recursion (choice of  $Q_0^2$ ) and therefore may be used for all  $Q$ , excepting again the very small  $Q^2$  region. Figure 2 shows values of  $f(x)$  which we obtained by a direct fit of Eq. (11) to the SLAC and Fermilab data,<sup>2,3</sup> with  $Q_0^2 = 3 \text{ GeV}^2$ . Again it is convenient to have a simple analytic form for  $f(x)$ ; we use

$$f(x) = a + bx + \epsilon/x \quad (12)$$

with  $a = 0.21324$ ,  $b = -0.97955$ , and  $\epsilon = 5.9 \times 10^{-4}$ . This parametrization generates the dashed curve shown in Fig. 2. The upward turn, owing to  $\epsilon \neq 0$ , is probably a reflection of the  $Q^2 \rightarrow 0$  behavior rather than deep-inelastic scale breaking. In any case this feature has no effect on our neutrino calculations since it occurs at very high  $\omega$ .

The quality of the fits obtained with logarithmic [Eq. (9)] and power [Eq. (11)]  $Q^2$  dependence is very similar. In Fig. 3 we show examples of our fits to  $B_L$  and  $B_P$ . The overall  $\chi^2$  is the same for the two displayed fits. Obviously one cannot say that experiment favors one over the other. We

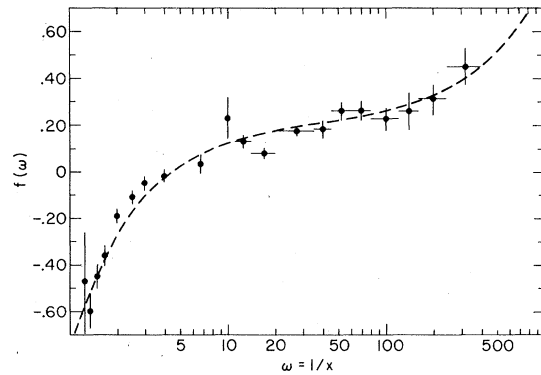


FIG. 2. The quantity  $f(\omega=1/x)$  vs  $\omega$  for power scale breaking, Eq. (11). The data are obtained from Ref. 2 ( $\omega \leq 10$ ), and Ref. 3 ( $\omega > 10$ ), as described in text. The curve represents our fit, Eq. (12), with  $Q_0^2 = 3 \text{ GeV}^2$ .

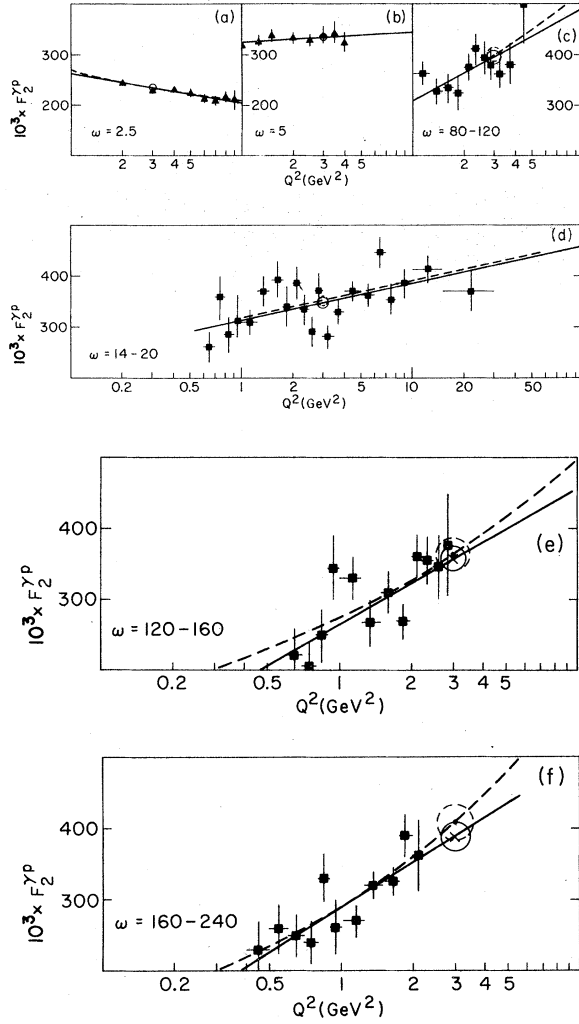


FIG. 3.  $F_2^{\gamma p}(Q^2)$  for different  $\omega = 1/x$  bins. The data are from Ref. 2 [ $\omega \leq 10$ , Figs. 3(a), 3(b)] and from Ref. 3 [ $\omega > 10$ , Figs. 3(c), 3(d), 3(e), 3(f)]. The results of logarithmic and power of  $Q^2$  fits are shown as solid and broken line, respectively. The centers of the circles show the values for  $F_2^{\gamma p}(Q_0^2 = 3 \text{ GeV}^2)$  from the fits with the radii representing the errors.

emphasize, as discussed above, that in both fits the quantity  $Q_0$  has no fundamental significance. It simply serves as a reference point for writing formulas; no experimental predictions would change if we changed  $Q_0$ . [Note, however, that the parameter  $\Lambda$  in Eq. (9) does have real significance.]

### III. DEEP-INELASTIC NEUTRINO SCATTERING

For the charged-current case we have, again dropping terms of order  $M_N^2/Q^2$ ,

$$\frac{d^2\sigma^{\nu/\bar{\nu}}}{dx dy} = \frac{G^2 M_N E}{\pi} [xy^2 F_1^{\nu/\bar{\nu}}(x, Q^2) + (1-y) F_2^{\nu/\bar{\nu}}(x, Q^2) \mp xy(1 - \frac{1}{2}y) F_3^{\nu/\bar{\nu}}(x, Q^2)], \quad (13)$$

where  $x$  and  $y$  are defined as before and the  $F_i^{\nu/\bar{\nu}}(x, Q^2)$  are the standard structure functions for the  $V \mp A$  weak charged currents.

The statistical quality of inelastic neutrino data does not yet permit systematic presentation of experimental results directly in terms of the variables  $Q^2$  and  $x$  which are natural for a structure function analysis. Instead, most of the available neutrino data<sup>15-21</sup> is reported as a function of  $x$  and  $y$  for fixed incoming neutrino energy  $E$ . This means that scale breaking, i.e., the  $Q^2$  dependence of the structure functions, is revealed as an energy dependence via the kinematic relation  $Q^2 = 2M_N xyE$ . Often only the  $x$  and/or  $y$  moments, calculated at fixed  $E$ , are presented. This complicates comparison to deep-inelastic  $eN$  and  $\mu N$  results, since constant  $E$  moments contain contributions from a range of  $Q^2$  including small  $Q^2$  values. For quantities which are obtained by integrating over  $x$  at fixed  $E$ , the energy dependence owing to scale breaking will always enter via the combination  $yE$ . We will indicate this explicitly in our formulas below.

Equation (13) may be rewritten

$$\begin{aligned} \frac{d^2\sigma^{\nu/\bar{\nu}}}{dx dy} &= \frac{G^2 M_N E}{\pi} 2xF_1^{\nu/\bar{\nu}}(x, Q^2) \\ &\times [1 - [1 \mp \mathcal{R}^{\nu/\bar{\nu}}(x, Q^2)](y - \frac{1}{2}y^2) \\ &+ \mathcal{R}(x, Q^2)(1-y)], \end{aligned} \quad (14)$$

where

$$\mathcal{R}^{\nu/\bar{\nu}}(x, Q^2) = -\frac{x F_3^{\nu/\bar{\nu}}(x, Q^2)}{2xF_1^{\nu/\bar{\nu}}(x, Q^2)} \quad (15)$$

and

$$\mathcal{R}^{\nu/\bar{\nu}}(x, Q^2) = \frac{F_2^{\nu/\bar{\nu}}(x, Q^2)}{2xF_1^{\nu/\bar{\nu}}(x, Q^2)} - 1. \quad (16)$$

If we integrate Eq. (14) over  $x$  at fixed  $E$  and  $y$ , we have

$$\begin{aligned} \frac{d\sigma^{\nu/\bar{\nu}}}{dy} &= \frac{G^2 M_N E}{\pi} \left( \int_0^1 dx 2xF_1^{\nu/\bar{\nu}}(x, 2M_N xyE) \right) \\ &\times \{1 - [1 \mp \mathcal{B}^{\nu/\bar{\nu}}(yE)](y - \frac{1}{2}y^2) \\ &+ \mathcal{R}^{\nu/\bar{\nu}}(yE)(1-y)\}, \end{aligned} \quad (17)$$

where

$$\mathcal{B}^{\nu/\bar{\nu}}(yE) = -\frac{\int_0^1 dx x F_3^{\nu/\bar{\nu}}(x, 2M_N xyE)}{\int_0^1 dx 2xF_1^{\nu/\bar{\nu}}(x, 2M_N xyE)} \quad (18)$$

and

$$R^{\nu/\bar{\nu}}(yE) = \frac{\int_0^1 dx F_2^{\nu/\bar{\nu}}(x, 2M_N yE)}{\int_0^1 dx 2xF_1^{\nu/\bar{\nu}}(x, 2M_N yE)} - 1. \quad (19)$$

It is important to note that when scaling is violated the  $y$  dependence of  $d\sigma^{\nu/\bar{\nu}}/dy$  is more complicated

than that given by the simple polynomial factors in Eq. (17). (This is discussed in detail in Sec. III E below.)

In the quark-parton model the structure functions can be readily expressed in terms of quark distributions. For an isoscalar target (equal number of protons and neutrons) these expressions take the form

$$F_1^{\nu}(x, Q^2) = \frac{1}{2}[u(x, Q^2) + d(x, Q^2) + \bar{u}(x, Q^2) + \bar{d}(x, Q^2) + 2\theta(2M_N Ey(1-x) - W_c^2)s(\xi_c, Q^2)]\cos^2\theta_c \\ + \frac{1}{2}[\bar{u}(x, Q^2) + \bar{d}(x, Q^2) + 2s(x, Q^2) + \theta(2M_N Ey(1-x) - W_c^2)[d(\xi_c, Q^2) + u(\xi_c, Q^2)]]\sin^2\theta_c, \quad (20)$$

$$F_2^{\nu}(x, Q^2) = (1 + R^{\nu})([x[u(x, Q^2) + d(x, Q^2) + \bar{u}(x, Q^2) + \bar{d}(x, Q^2)] + 2\xi_c\theta(2M_N Ey(1-x) - W_c^2)s(\xi_c, Q^2)]\cos^2\theta_c \\ + [x[\bar{u}(x, Q^2) + \bar{d}(x, Q^2) + 2s(x, Q^2)] + \xi_c\theta(2M_N Ey(1-x) - W_c^2)[d(\xi_c, Q^2) + u(\xi_c, Q^2)]]\sin^2\theta_c), \quad (21)$$

and

$$F_3^{\nu}(x, Q^2) = -[u(x, Q^2) + d(x, Q^2) - \bar{u}(x, Q^2) - \bar{d}(x, Q^2) + 2\theta(2M_N Ey(1-x) - W_c^2)s(\xi_c, Q^2)]\cos^2\theta_c \\ - [-\bar{u}(x, Q^2) - \bar{d}(x, Q^2) + 2s(x, Q^2) + \theta(2M_N Ey(1-x) - W_c^2)[d(\xi_c, Q^2) + u(\xi_c, Q^2)]]\sin^2\theta_c, \quad (22)$$

where  $\sin^2\theta_c = 0.05$ ,  $W_c = 3$  GeV,  $\xi_c = x(1 + m_c^2/Q^2)$ , and  $m_c = 1.5$  GeV. [For antineutrinos the corresponding expressions are obtained by the substitutions  $(u, d, s) \rightarrow (\bar{u}, \bar{d}, \bar{s})$  and in addition the overall sign of  $F_3^{\bar{\nu}}$  should be changed.] The last three parameters control the turn-on of charm production as discussed in Ref. 22. We have chosen to use a  $\theta$ -function cutoff and the "slow" scaling variable  $\xi_c$ , in spite of the fact that this undoubtedly neglects dynamical effects, because we have then all of the correct qualitative features: no charm production at low energies, a scaling charm contribution at high  $Q^2$ , and a transition between the two regimes with a scale set by  $m_c^2$ . Since the neutrino data we discuss below span the charm-threshold region it is important to have some description of this effect. Within the accuracy of present neutrino data a description in terms of  $\xi_c$  seems quite adequate.

In making predictions for neutrino and antineutrino scattering we require a set of quark-parton distributions. We make use of three different sets: those of Chu and Gunion, of Fox, and of Dao *et al.*<sup>5</sup> These distributions are used with the following modifications. We leave the  $u$  and  $d$  distributions unchanged, retain the form of the  $s$  and  $\bar{s}$  distributions, choose a normalization such that  $s$  is one half of  $\bar{u}$ , and neglect the charm content of the sea. We also assume that the above distributions are appropriate for  $Q^2 = Q_0^2 = 3$  GeV<sup>2</sup>. We find that our results are quite insensitive to the particular choice of quark-parton distributions.

We choose for both neutrinos and antineutrinos a constant value  $R = 0.14$  as suggested by electroproduction,<sup>11</sup> except when specifically stated otherwise. Since almost all neutrino experiments are analyzed assuming  $R = 0$ , we must on occasion correct for this.

To compare our results with neutrino data we must first understand and include the acceptance cuts particular to each experiment. We study here results obtained in bubble chambers: Gargamelle (GGM),<sup>15</sup> the 15 ft bubble chamber at Fermilab (FIMS),<sup>16</sup> and the Big European Bubble Chamber (BEBC)<sup>17</sup>, as well as results obtained from counter experiments: the Harvard-Pennsylvania-Wisconsin-Fermilab (HPWF)<sup>18</sup> and the Caltech-Fermilab-Rockefeller (CFR)<sup>19,20</sup> collaborations working at Fermilab, and the CERN-Dortmund-Heidelberg-Saclay-Bologna (CDHS)<sup>21</sup> collaboration at CERN. Results from all of these experiments are shown in Figs. 4-10. However, since the experimental acceptance, and in the case of  $B(E)$  even the definition of the quantity presented, differs from one experiment to another, the results from different groups cannot always be compared directly. We therefore study the various experiments separately when necessary.

#### A. Total cross sections (Fig. 4)

For exact scaling the "slopes"  $\sigma^{\nu}/E$  and  $\sigma^{\bar{\nu}}/E$  are constants. As Fig. 4 shows, the slope of the neutrino cross section is higher in the Gargamelle

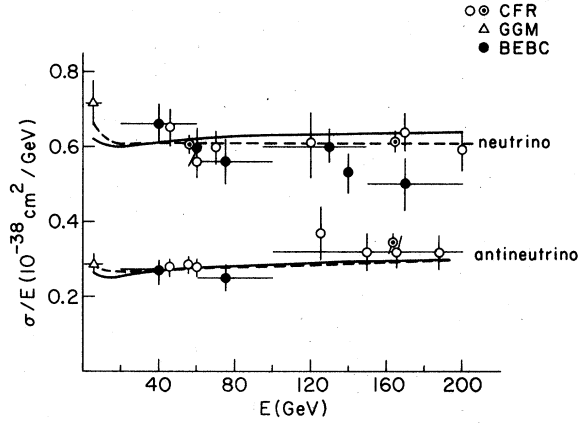


FIG. 4. The cross-section "slopes"  $\sigma^\nu/\bar{\nu}/E$  vs incident energy. The data are from CFR (Ref. 20; the dotted circles represent high- and low-energy averages of the same data), GGM (Ref. 15), and BEBC (Ref. 17). Our predictions for power and logarithmic  $Q^2$  dependence are shown as broken and solid curves, respectively.

low-energy region<sup>15</sup> than that measured by CFR<sup>20</sup> and BEBC<sup>17</sup> at  $E \geq 50$  GeV where the data indicates either a constant behavior or a slight decrease. Strictly speaking, given the large scatter and statistical errors of the present measurements even a constant behavior everywhere is not ruled out. (Note that these data as well as the data in Fig. 5 are corrected for acceptance losses and therefore may be compared directly to one another.)

Our curve for power-type scale breaking follows the trend of neutrino data very well, showing a rapid drop at low energy,  $5 < E < 15$  GeV followed by a flat plateau. The behavior at low  $E$  can be understood when one realizes that  $\langle Q^2 \rangle$  increases from 1.5 to 3.5  $\text{GeV}^2$  over this energy interval (Fig. 5) and that  $(Q^2/Q_0^2)^f$  with  $f < 1$  varies rapidly for  $Q^2/Q_0^2 \leq 1$  and slowly for  $Q^2/Q_0^2$  large. The curve for logarithmic scale breaking shows a small drop in the region just above the Gargemelle data point and then switches over to a gradual rise with increasing energy.

The antineutrino data displayed in Fig. 4 suggest a constant "slope" for  $E \leq 80$  GeV followed by a slight rise above this energy. Again, an overall constant behavior is not ruled out by experiment. We see that the predictions of both power-type and logarithmic scale breaking follow the trend of the antineutrino data very well. The slight rise with energy which both predict is due to the fact that the rising antiquark contribution which is flat in  $y$ , is significant addition to the  $(1-y)^2$  contribution of the valence quarks in the antineutrino cross section. The analogous effect

in  $\sigma^\nu/E$  is much smaller since the antiquark contribution is instead suppressed by  $(1-y)^2$  compared to the valence-quark terms which are flat in  $y$ . The key conclusion we draw from Fig. 4 is that although scale breaking produces energy-dependent "slopes" for the neutrino and antineutrino cross sections, the variations when calibrated by deep-inelastic electron and muon scattering are quite small for either power-type or logarithmic scale breaking. Uncertainties in the present data greatly exceed the expected changes in  $\sigma/E$  with energy. We have tested the sensitivity of these conclusions to the choice of parton-model distributions and find that the changes are much smaller than the scatter of the data. Setting  $R=0$  in our fits produces noticeable changes in the  $\sigma/E$  slopes, lowering them 10–15% for antineutrino and 5–10% for neutrino.

#### B. Mean squared momentum transfer (Fig. 5)

The data for  $\langle Q^2 \rangle = 2M_N E \langle xy \rangle$  are still very scarce at high energies for both neutrinos and antineutrinos.<sup>15–17</sup> However, the experimental trend shown in Fig. 5 is well approximated by both the

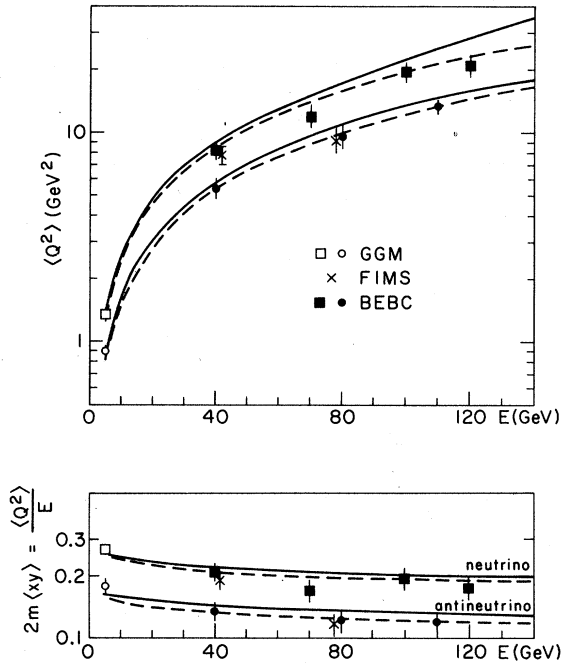


FIG. 5. Mean momentum transfer squared, scaled  $\langle Q^2 \rangle/E$  and unscaled  $\langle Q^2 \rangle$  for  $\nu/\bar{\nu}$  vs incident energy. The data are from GGM (Ref. 15), FIMS (Ref. 16) and BEBC (Ref. 17). Fits from power and logarithmic  $Q^2$  dependence are shown as broken and solid curves, respectively.

power and logarithmic scale-breaking forms we obtained from electroproduction. As remarked above, this trend supports our understanding of the behavior of  $\sigma^\nu/E$  at low energy. Again, the predicted decrease of  $\langle Q^2 \rangle / 2M_N E$  with increasing energy is insensitive to the choice of parton densities. We hope that  $\langle Q^2 \rangle$  will be studied further experimentally.

### C. The $\sigma^{\bar{\nu}}/\sigma^\nu$ ratio (Fig. 6)

There exists considerably more data for the cross-section ratio  $R_c = \sigma^{\bar{\nu}}/\sigma^\nu$  than for the individual cross sections themselves. We show these data in Fig. 6 but emphasize that the results from different experiments cannot be compared directly in some cases because of different experimental cuts. The low energy GGM<sup>15</sup> point and the high energy CFR<sup>20</sup> and BEBC<sup>17</sup> points are corrected to 100% acceptance as in Fig. 4.

The CDHS data<sup>21</sup> are uncorrected for an angular acceptance cut  $\theta \leq 400$  mrad and minimum muon momentum cut  $p_\mu \geq 5$  GeV. The  $p_\mu$  requirement translates to  $y \leq 1 - 5/E$  (GeV), which cuts out the high- $y$  region, a region more important for neutrinos than antineutrinos; this gives an apparent  $R_c$  slightly higher than the true value.

The HPWF points<sup>18</sup> shown in Fig. 6 have been corrected by this group for experimental cuts

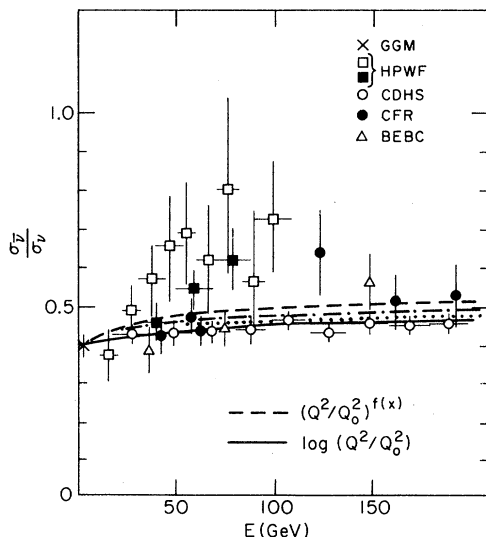


FIG. 6. Ratio of antineutrino and neutrino total charged-current cross sections. Data are from HPWF (Ref. 18), CDHS (Ref. 21), CFR (Ref. 20), and BEBC (Ref. 17). Fits for power and logarithmic  $Q^2$  dependence are shown as broken and solid curves, respectively. The dotted and dash-dotted curves are QCD asymptotic-freedom fits from Ref. 25 and Ref. 24, respectively.

and inefficiencies by a procedure which assumed scaling. The two sets of HPWF points (open and solid squares) shown in Fig. 6 were obtained using different flux normalizations. Our curves favor the lower version of the HPWF data but we feel no clear statement can be made. Our attempt to include the HPWF acceptance cuts does not reproduce the trend shown in Fig. 6 for this experiment. We hope that a new analysis of these data will become available.

Our curves shown in Fig. 6 for both power-type and logarithmic scale breaking are computed assuming *full acceptance*. The two types of  $Q^2$  dependence produce slightly different  $R_c(E)$ , but both results are compatible with the combined GGM, CFR, and BEBC data except for one high CFR point at 125 GeV. When we increase<sup>23</sup>  $R = \sigma_S/\sigma_T$  from 0.14 to 0.25 we find a 5–10% increase in  $R_c$ . Conversely setting  $R=0$  in our fits, we obtain an  $R_c$  value 5–10% lower than the  $R_c$  shown in Fig. 6 which corresponds to  $R=0.14$ . Again different quark-parton-model distributions give very similar results. Also shown in Fig. 6 are two curves calculated for full acceptance using the formalism of asymptotic freedom. The dash-dotted line is the “ $x$  fit” of Fox<sup>24</sup> and the dotted line is the “ASF fit” of Buras.<sup>25</sup> The similarity to our results is notable.

When we include the CDHS acceptance cuts (as discussed previously) in our predicted curves, we obtain an  $R_c$  which for  $E < 100$  GeV lies 5% above the values indicated in Fig. 6; above 100 GeV the curves with cuts approach the total acceptance curves shown in Fig. 6. These predictions lie slightly higher than the CDHS results.<sup>21</sup>

We conclude that the predicted behavior of  $R_c$  is consistent with the GGM,<sup>15</sup> BEBC,<sup>17</sup> CFR,<sup>20</sup> and CDHS<sup>21</sup> data for either power-type or logarithmic scale breaking parametrizations. As with other observables, the scale breaking effects are predicted not to be large.

### D. Mean value of $y$ (Figs. 7–9)

In Fig. 7 we show all of the available data<sup>16–21</sup> for  $\langle y \rangle^\nu$  and  $\langle y \rangle^{\bar{\nu}}$  along with our scale breaking predictions calculated *without* acceptance cuts. Since our logarithmic and power-type predictions agree within 3% over the entire energy range their difference is too small to show in Fig. 7; the solid curves shown in Fig. 7 apply to either model. Also shown in Fig. 7 are the predictions of the same two asymptotic-freedom calculations illustrated in Fig. 6. Setting  $R=0$  produces a higher  $\langle y \rangle$ . The effect is 10–15% for antineutrinos and ~2% for neutrinos.

The sensitivity of model predictions to experi-

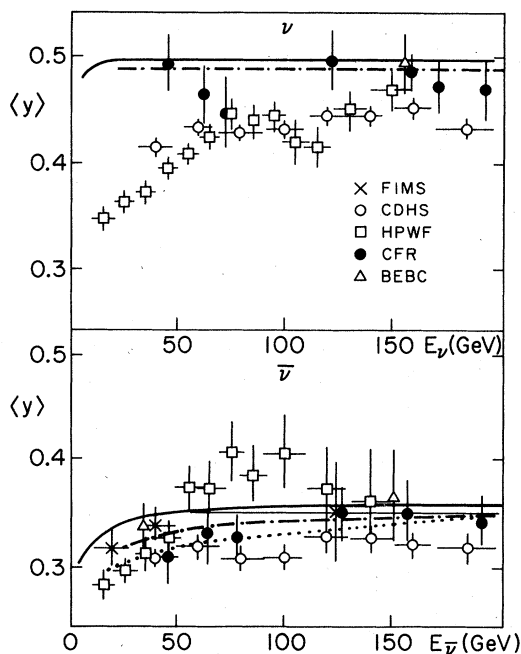


FIG. 7. Mean value of  $y$  for  $\nu/\bar{\nu}$ . Data are from FIMS (Ref. 16), CDHS (Ref. 21), HPWF (Ref. 18), CFR (Ref. 20), and BEBC (Ref. 17). The solid curve represents our predictions (logarithmic and power, see text), without acceptance cuts. The dotted and dash-dotted curves are QCD asymptotic-freedom fits from Refs. 25 and 24, respectively.

mental cuts is well illustrated by  $\langle y \rangle$ . Figure 7 shows good agreement between our predictions and the bubble-chamber data (FIMS<sup>16</sup> and BEBC)<sup>17</sup> and partial agreement with the CFR counter data<sup>20</sup> all of which correspond to 100% acceptance. The variation in  $\langle y \rangle$  below 50 GeV is mostly due to the charm threshold whereas the slight variation above this energy is due to genuine asymptotic effects.

In Fig. 8 we show  $\langle y \rangle$  from the CDHS experiment<sup>21</sup> together with three model predictions: (a) our scale breaking predictions (*power or logarithmic*) with no cuts (broken line), (b) our predictions but with the CDHS cuts  $\theta_\mu \leq 400$  mrad and  $p_\mu \geq 5$  GeV (solid line), and (c) no scale breaking but with experimental cuts as in (b) and  $B = \text{const} = 0.8$  (dash-dotted line). All three curves and the data have the additional cut  $x \leq 0.6$ . This latter restriction has only a very weak effect.

We see that the influence of the muon-momentum cut is large and in the correct direction to improve agreement between our predictions and experiment. This effect is not big enough, however. The predictions remain too high compared to the CDHS data. However, there are puzzling features

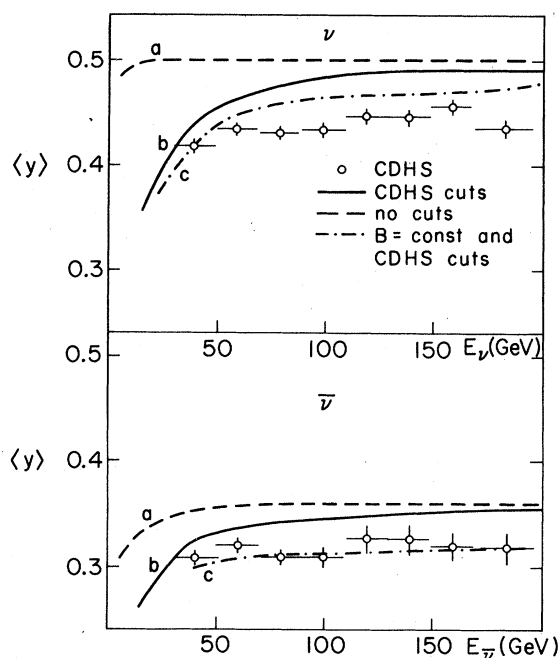


FIG. 8. Mean value of  $y$  for  $\nu/\bar{\nu}$  obtained by CDHS (Ref. 21). Curves are our predictions for (a) scale breaking, with no acceptance cuts (b), same but with CDHS acceptance cuts (Ref. 21), and (c) no scale breaking, but acceptance cuts are included and  $B = 0.8$ .

of the published CDHS results for  $\langle y \rangle$ . As the dash-dotted curve in Fig. 8 shows, the value of  $\langle y \rangle$  for antineutrinos is consistent with a scaling fit with  $B = 0.8$ , but the same picture is not consistent with the neutrino results for  $\langle y \rangle$ . Thus unless the published description of the experimental cuts is incomplete or unknown systematic effects are at work, one will have to consider unconventional processes to cause  $B'$  to be substantially smaller than  $B''$ . (See Sec. IIIE below.) This feature of the published data needs clarification.

Finally, we show in Fig. 9 the HPWF results<sup>18</sup> and our model prediction without cuts (broken line) and with the experimental cuts  $p_\mu \geq 4$  GeV,  $\theta_\mu \leq 225$  mrad, and  $Q^2 > 1$  GeV<sup>2</sup> or  $W > 1.6$  GeV (solid line). As in Fig. 8 all curves and data also contain the mild cut,  $x \leq 0.6$ . As expected, the major effect of the muon cut is a strong decrease of  $\langle y \rangle$  at low energy which improves but does not bring about agreement between our predictions and the HPWF data. However, because there are apparently large efficiency corrections for high  $y$  events ( $y \geq 0.6$ ) for the HPWF apparatus at low energies,<sup>18</sup> the remaining disagreement below 50 GeV is probably not serious. On the other hand we have no way of accounting for the very

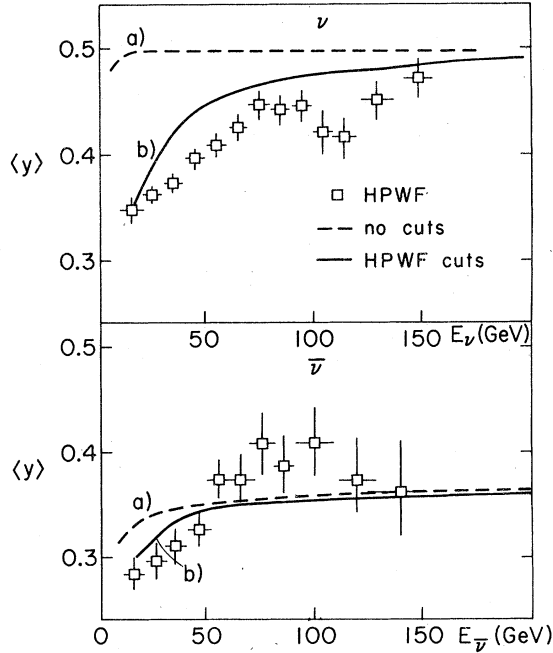


FIG. 9. Mean value of  $y$  for  $\nu/\bar{\nu}$  obtained by HPWF (Ref. 18). Curves are our predictions for (a) scale breaking with no acceptance cuts and (b) same but with HPWF acceptance cuts (Ref. 18).

high values of  $\langle y \rangle^{\bar{\nu}}$  observed in the interval  $50 \text{ GeV} \leq E \leq 100 \text{ GeV}$  nor the glitches observed in  $\langle y \rangle^{\nu}$  above  $100 \text{ GeV}$ . Some of these effects may be systematic as Fig. 7 suggests.

The comparison of  $\langle y \rangle$  from various experiments with our quark-parton scale breaking models is inconclusive. Since we have seen how sensitive the results for  $\langle y \rangle$  are to the acceptances of a given experiment, the situation will not be clarified until the detailed cuts and corrections which have been made in various experiments are fully stated and published, and the consistency or inconsistency of the different neutrino experiments finally settled.

#### E. Shape parameter $B$ (Fig. 10)

When scaling is exact and  $R=0$ , the  $y$  dependence of  $d\sigma^{\nu}/dy$  ( $d\sigma^{\bar{\nu}}/dy$ ) is characterized by a single constant  $B^{\nu}$  ( $B^{\bar{\nu}}$ ) defined as in Eq. (18) except that there is no energy dependence. This constant then reflects the fraction of the target momentum carried by antiquarks. For an isoscalar target and in the kinematic region well above the charm threshold, one has (independent of  $\theta_C$ )

$$\Delta B \equiv B^{\nu} - B^{\bar{\nu}} = \frac{4 \int_0^1 dx x(s-c)}{\int_0^1 dx x(u+\bar{u}+d+\bar{d}+2s+2c)} \quad (23)$$

[Note that in writing Eq. (23) we have included charmed-quark and antiquark contributions which in our numerical calculations and previous formulas were set equal to zero.]

We see from Eq. (23) that  $\Delta B$  is expected to be nonzero except for the special situation in which strange and charmed quarks carry equal amounts of the nucleon's momentum [e.g. SU(4) sea]. At presently accessible  $Q^2$  the difference  $\Delta B$  should be small, however, since only the denominator in Eq. (23) contains the large valence contributions. For the kinematic region close to the charm threshold the expression for  $\Delta B$  is slightly more complicated but, because it contains an explicit factor of  $\sin^2 \theta_C$ , a small but in general nonzero  $\Delta B$  will result. Thus on rather general theoretical grounds we expect that  $\Delta B \neq 0$  but  $|\Delta B| \ll (B^{\nu} + B^{\bar{\nu}})$  throughout the kinematic range of  $Q^2$  now available.

The experimental situation regarding  $B^{\nu/\bar{\nu}}$  is rather complex as we now discuss. Essentially all experimental groups assume in their analyses that  $B^{\nu} = B^{\bar{\nu}}$ ; this is reasonable given the present errors unless new quarks and/or new currents are present. When scaling is violated, the  $B$  parameter [see Eq. (18)] picks up a  $y$  dependence through  $Q^2 \sim Ey$ . Since various experiments handle this problem differently, one must take their particular methods into account, as well as the possible presence of an  $R(1-y)$  term, when comparing the prediction for  $B$  of any scale breaking model with experimental results.

The BEBC collaboration<sup>17</sup> defines in their

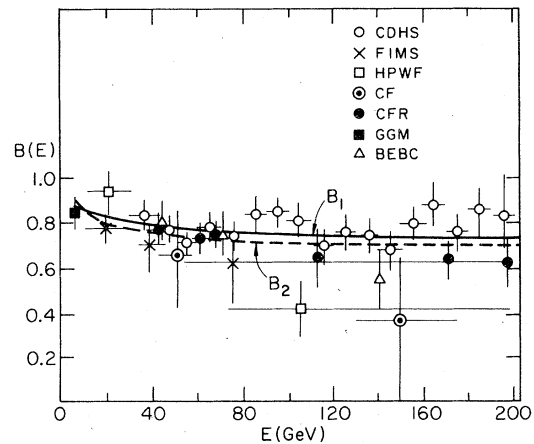


FIG. 10. The shape parameters  $B_1$ ,  $B_2$ , and  $B'$  (see text). Data are  $B'$  from CDHS (Ref. 21), FIMS (Ref. 16), HPWF (Ref. 18);  $B_2$  from CF (Ref. 19) and CFR (Ref. 20);  $B_1$  from GGM (Ref. 15) and BEBC (Ref. 17). Our predictions for  $B_1$  and  $B_2$  (for either power-type or logarithmic scale breaking) are represented by the solid and dashed curves, respectively.

analysis a parameter  $B_1$ ,

$$B_1 = 2 \left( \frac{\sigma^\nu - \sigma^{\bar{\nu}}}{\sigma^\nu + \sigma^{\bar{\nu}}} \right). \quad (24)$$

This is the only analysis which stresses that, because of the  $y$  dependence of  $B$  as defined by Eq. (18), the procedure of fitting the experimental  $y$  distribution with a constant  $B$  to

$$\frac{d\sigma^{\nu/\bar{\nu}}}{dy} \propto [1 - (1 \mp B^{\nu/\bar{\nu}})y + (1 \mp B^{\nu/\bar{\nu}})y^2/2] \quad (25)$$

gives a different value of  $B$  than Eq. (24). The BEBC<sup>17</sup> and GGM<sup>15</sup> data points are shown in Fig. 10 as defined by Eq. (24). Also shown are our predictions for  $B_1(E)$  (solid curve). As in Figs. 7–9, the results for power-type and logarithmic scale breaking differ by so little ( $\leq 3\%$ ) that we have represented them by a common curve.

The CFR collaboration employs a somewhat different analysis. They first note that for exact scaling and  $R=0$  the numerator and denominator of Eq. (18) can each be written in two equivalent forms. Namely for the numerator,  $f_3 = \int dx x F_3(x)$ , one has

$$f_3 = \frac{3}{2} C (\sigma^\nu - \sigma^{\bar{\nu}}) / E \quad (26)$$

and alternatively

$$f_3 = \frac{12}{5} C (\langle y \rangle^\nu \sigma^\nu - \langle y \rangle^{\bar{\nu}} \sigma^{\bar{\nu}}) / E, \quad (27)$$

where

$$C = \pi / (G^2 M_N) \quad (28)$$

and similarly for the denominator,  $f_2 = \int dx x F_2(x)$ ,

$$f_2 = \frac{3}{4} C (\sigma^\nu + \sigma^{\bar{\nu}}) / E \quad (29)$$

and

$$f_2 = \frac{12}{7} C (\langle y \rangle^\nu \sigma^\nu + \langle y \rangle^{\bar{\nu}} \sigma^{\bar{\nu}}) / E. \quad (30)$$

In the presence of scaling violations all four of the observables  $\sigma^{\nu,\bar{\nu}}/E$  and  $\langle y \rangle^{\nu,\bar{\nu}}$  develop a weak energy dependence and the equation pairs (26), (27) and (29), (30) are no longer equivalent. Using just the total cross sections would give the quantity  $B_1(E)$  discussed above with the BEBC results. Instead, CFR do a best fit to Eqs. (26) and (27) to determine a quantity we call  $\bar{f}_3(E)$  and similarly do a best fit to Eqs. (29) and (30) to determine a second quantity  $\bar{f}_2(E)$ . In terms of these one may define

$$B_2(E) \equiv -\bar{f}_3(E) / \bar{f}_2(E). \quad (31)$$

The CFR values for this quantity are indicated in Fig. 10.

For the case in which the errors of  $\sigma^{\nu,\bar{\nu}}$  and  $\langle y \rangle^{\nu,\bar{\nu}}$  are of the same size, this procedure corresponds to

$$B_2(E) = \frac{561}{89} \frac{8(\sigma^\nu - \sigma^{\bar{\nu}}) + 5(\langle y \rangle^\nu \sigma^\nu - \langle y \rangle^{\bar{\nu}} \sigma^{\bar{\nu}})}{32(\sigma^\nu + \sigma^{\bar{\nu}}) + 7(\langle y \rangle^\nu \sigma^\nu + \langle y \rangle^{\bar{\nu}} \sigma^{\bar{\nu}})}. \quad (32)$$

When the errors differ, the usual  $\chi^2$  minimization gives a rather longer expression for  $B_2(E)$ .

Figure 10 shows our predictions (dashed line) for the quantity  $B_2$  calculated from Eq. (32). We note that  $B_2$  lies systematically below  $B_1$  except at very low energies. Although the difference between  $B_1$  and  $B_2$  is not large, Fig. 10 illustrates the important fact that in the future when high-precision neutrino data becomes available, great care will be necessary in defining the  $B$  parameter, especially if scaling violations are to be studied as a function of energy.<sup>26</sup>

The GGM,<sup>15</sup> BEBC,<sup>17</sup> and CFR<sup>20</sup> results agree with our prediction for  $E \leq 80$  GeV and, given the large errors, also at higher energies. We note, however, that above 80 GeV the BEBC and CFR data systematically lie below the predictions for  $B_1$  and  $B_2$ .

In this connection it is interesting to consider the effect of  $R = \sigma_s / \sigma_T$  on the determination of the  $B$  parameter. For this purpose we may neglect scale breaking corrections and assume  $B^\nu = B^{\bar{\nu}} \equiv B$ . A nonzero value of  $R$  introduces an additional  $(1-y)$  term in both  $d\sigma/dy$  and  $d\sigma^{\bar{\nu}}/dy$ . With the help of Eq. (17) it is easy to show

$$B_1 = B / (1 + \frac{3}{4}R), \quad (33)$$

where  $B_1$  is obtained from the total cross sections via Eq. (24) and  $B$  from Eq. (18). We see that for a given  $B = -\int dx x F_3 / \int dx x F_2$ , the value of  $B_1$  is 10% higher when we assume  $R=0$  than is the case for  $R=0.14$ . Thus decreasing the value of  $R$  used in calculating the curve for  $B_1$  shown in Fig. 10 will tend to worsen the agreement between our predictions and the BEBC and CFR data. The same effect occurs for  $B_2$ .

The CDHS,<sup>21</sup> FIMS,<sup>16</sup> and HPWF<sup>18</sup> published values of the  $B$  parameter correspond neither to  $B_1$  nor  $B_2$ . Instead, these groups report the best fit value for the parameter obtained by fitting Eq. (18) to their experimental  $y$  distributions, ignoring the  $yE$  dependence of  $B$  which will be present with scale breaking. For purposes of identification we will refer to parameter  $B$  obtained in this manner as  $B'$ . This procedure, while adequate for identifying the presence or absence of scale breaking, is not suitable for quantitative studies since the  $E$  dependence observed in  $B'$  has no clear significance.

The CDHS,<sup>21</sup> FIMS,<sup>16</sup> and HPWF<sup>18</sup> values for  $B'$  are shown in Fig. 10. The FIMS points<sup>16</sup> are for  $B'^{\bar{\nu}}$ , the CDHS<sup>21</sup> and HPWF<sup>18</sup> points are obtained under the assumption  $B'^\nu = B'^{\bar{\nu}}$ . It is virtually impossible to show model predictions for

the quantity  $B'$ , since the experimental values correspond to fitting the data with a functional form which is not always consistent with theory or the data itself.<sup>18</sup> Thus the comparison of the CDHS, FIMS, and HPWF data points in Fig. 10 with either of the curves in Fig. 10 is only qualitative and disagreement, when present, has no clear significance. It is clear from Fig. 10, moreover, that the present situation for  $B'$  is dominated by disagreements between the various experiments, all of which report to have used the same method to obtain  $B'$ . This needs to be clarified. We advocate that experimental results in the future not be presented by means of the parameter  $B'$ , since, as described above, it has no clear theoretical meaning.

#### IV. SUMMARY

We have examined scaling violations in charged-current neutrino and antineutrino inelastic scattering by means of a phenomenological procedure using input data from muon and electron scattering.<sup>2,3</sup> We conclude that in spite of the intellectual attractiveness of asymptotically free QCD the experimental data examined here do not yet demand it. Both power-type and logarithmic

scale-breaking forms give acceptable and similar descriptions in the presently studied energy region.<sup>15-21</sup> The global variables (i.e., those integrated over  $x$  and  $y$ )  $\sigma/E$ ,  $\langle y \rangle$ , and  $\langle Q^2 \rangle/E$ , for which the most experimental data is available,<sup>15-21</sup> are predicted to have only a very weak dependence on the neutrino (antineutrino) energy  $E$ . At present the experimental uncertainties permit only a qualitative confirmation of this energy dependence. Quantitative analysis will require very precise measurements of global variables or measurements of structure functions at fixed  $x$ , something which has only recently become a real possibility.<sup>26</sup>

#### ACKNOWLEDGMENTS

This work was supported in part by the National Science Foundation under Grant No. NSF 77-25279. We wish to thank Professor H. Anderson for providing us with detailed data on inelastic muon scattering and Dr. A. Buras, Dr. M. Mestayer, Professor F. Sciulli and Professor T. B. Kirk for helpful conversations. One of us (I.K.) wishes to thank NORDITA and the Physics Department of Tel Aviv University for their hospitality during parts of this work.

<sup>1</sup>G. Parisi and R. Petronzio, Phys. Lett. **62B**, 331 (1976); G. Altarelli, R. Petronzio, and G. Parisi, *ibid.* **63B**, 182 (1976); A. de Rújula, M. Georgi, and D. H. Politzer, Ann. Phys. (N.Y.) **103**, 315 (1977); R. M. Barnett, M. Georgi, and D. H. Politzer, Phys. Rev. Lett. **37**, 1313 (1976); M. Gluck, and E. Reya, Phys. Lett. **64B**, 169 (1976); Phys. Rev. D **14**, 3034 (1976); A. Buras and K. J. F. Gaemers, Phys. Lett. **71B**, 106 (1977); Nucl. Phys. **B132**, 249 (1978); A. Buras, *ibid.* **B125**, 125 (1977); I. Hinchliffe and C. Llewellyn Smith, Phys. Lett. **66B**, 281 (1977); Nucl. Phys. **B128**, 93 (1977); V. Barger *et al.*, Phys. Rev. D **14**, 1276 (1976); G. C. Fox, Nucl. Phys. **B134**, 269 (1978). Discussions of a more phenomenological nature have been given by G. Shaw, D. Faroughy, and P. Thomas, Phys. Rev. Lett. **38**, 1244 (1977); R. Kogerler and D. Schildknecht, Phys. Lett. **66B**, 461 (1977); P. H. Frampton and J. J. Sakurai, Phys. Rev. D **16**, 572 (1977); D. P. Roy *et al.*, Tata Institute report (unpublished); R. H. Graham, E. M. Haacke, and P. Savaria, Univ. of Toronto report (unpublished).

<sup>2</sup>J. S. Poucher *et al.*, Phys. Rev. Lett. **32**, 118 (1974); E. M. Riordan *et al.*, Phys. Lett. **52B**, 249 (1974); Phys. Rev. Lett. **33**, 561 (1976); Report No. SLAC-PUB-1634, 1975 (unpublished); R. E. Taylor, in *Proceedings of the 1975 International Symposium on Lepton and Photon Interactions at High Energies, Stanford, California*, edited by W. T. Kirk (SLAC, Stanford, 1976), p. 679.

<sup>3</sup>H. L. Anderson *et al.*, Phys. Rev. Lett. **37**, 4 (1976);

**38**, 1450 (1977); private communication on the combined results of Fermilab experiments E98 and E398.

<sup>4</sup>S. L. Glashow, J. Iliopoulos, and L. Maiani, Phys. Rev. D **2**, 1285 (1970).

<sup>5</sup>G. Chu and J. Gunion, Phys. Rev. D **10**, 3672 (1974); G. C. Fox, Nucl. Phys. **B131**, 107 (1977). (The distributions are given here at  $Q^2=2 \text{ GeV}^2$ ; we have adjusted for this in our fits.) F. T. Dao *et al.*, Phys. Rev. Lett. **39**, 1388 (1977).

<sup>6</sup>For a review, see H. D. Politzer, Phys. Rep. **14C**, 129 (1974).

<sup>7</sup>Wu-Ki Tung, Phys. Rev. Lett. **35**, 490 (1975); Phys. Rev. D **12**, 3613 (1975); P. Johnson and Wu-Ki Tung, Nucl. Phys. **B121**, 270 (1977); Phys. Rev. D **16**, 2769 (1977).

<sup>8</sup>Almost all of the work of Ref. 1 assumes  $Q^2$ -dependent quark-parton-model densities, since experiment clearly rules out factorization of the  $x$  and  $Q^2$ -dependences.

<sup>9</sup>C. G. Callan and D. Gross, Phys. Rev. Lett. **22**, 156 (1969).

<sup>10</sup>L. N. Hand, in *Proceedings of the International Symposium on Lepton and Photon Interactions at High Energies, Hamburg, 1977*, edited by F. Guthrod (DESY, Hamburg, 1977).

<sup>11</sup>E. M. Riordan *et al.* (Ref. 2).

<sup>12</sup>H. D. Politzer, Nucl. Phys. **B129**, R5 (1977).

<sup>13</sup>For a general review, see C. Llewellyn Smith, Phys. Rep. **3C**, 261 (1972).

<sup>14</sup>D. H. Perkins, P. Schreiner, and W. G. Scott, Phys.

- Lett. 67B, 347 (1977).
- <sup>15</sup>T. Eichten *et al.*, Phys. Lett. 46B, 281 (1973); H. Deden *et al.*, Nucl. Phys. B85, 269 (1975).
- <sup>16</sup>F. A. Nezrick, in *Proceedings of the Summer Institute on Particle Physics*, edited by M. C. Zipf (Stanford Linear Accelerator Center, Stanford, California, 1976); J. Berge *et al.*, Phys. Rev. Lett. 36, 639 (1976); Fermilab-IHEP-ITEP-Michigan Neutrino Group, Phys. Rev. Lett. 39, 382 (1977).
- <sup>17</sup>K. Schultze, in *Proceedings of the International Symposium on Lepton and Photon Interactions at High Energies, Hamburg, 1977* (Ref. 10); P. C. Bosetti *et al.*, Phys. Lett. 70B, 271 (1977).
- <sup>18</sup>A. Benvenuti *et al.*, Phys. Rev. Lett. 32, 125 (1974); 34, 597 (1975); 36, 1478 (1976); 37, 189 (1976); 39, 1095 (1976); B. Aubert *et al.*, *ibid.* 33, 984 (1974).
- <sup>19</sup>B. C. Barish *et al.*, Phys. Rev. Lett. 31, 656 (1973); 35, 1316 (1975); 38, 314 (1977); Caltech Report No. CALT-68-56 (unpublished).
- <sup>20</sup>B. C. Barish *et al.*, Phys. Rev. Lett. 39, 741 (1977); 39, 1595 (1977); Caltech Reports No. 68-606 and 68-607 (unpublished); F. Sciulli, in *Proceedings of the International Symposium on Lepton and Photon Interactions at High Energies, Hamburg, 1977* (Ref. 10).
- <sup>21</sup>M. Holder *et al.*, Phys. Rev. Lett. 39, 433 (1977).
- <sup>22</sup>R. M. Barnett, Phys. Rev. 36, 1163 (1976); Phys. Rev. D 14, 70 (1976); H. Georgi and D. Politzer, Phys. Rev. Lett. 36, 1281 (1976); O. Nachtmann, Nucl. Phys. B63, 237 (1973); B78, 455 (1974).
- <sup>23</sup>L. N. Hand (Ref. 10); H. L. Anderson *et al.*, Phys. Rev. Lett. 40, 1061 (1978); H. Mestayer, private communication.
- <sup>24</sup>G. C. Fox, Ref. 1.
- <sup>25</sup>A. Buras, Ref. 1.
- <sup>26</sup>Data for  $B$  as a function of  $x$  and  $Q^2$ , Eq. (15), are still scarce. However, in addition to earlier data of Ref. 16, new data have recently been analyzed by the BEBC collaboration [B. Tallini, preliminary results presented at 1978 Purdue Neutrino Conference (unpublished)]. These data give further support to QCD through the analysis of moments of the structure functions.